Transition Met Chem (2013) 38:801–809
DOI 10.1007/s11243-013-9752-2

Synthesis, structure, and electronic calculations of group VII substituted pyridazines

C. A. Snyder · N. C. Tice · J. B. Maddox · J. O. E. Young · M. G. Mazzotta · B. D. Garabato · J. W. Evans · L. A. Dopierala · S. A. Shah · Z. A. Claytor · A. C. Smith

Received: 3 June 2013 / Accepted: 26 July 2013 / Published online: 10 August 2013

Abstract A series of 5,6-fused ring cyclopentadienyl tricarbonyl manganese and rhenium complexes, $[M(CO)_3\text{-}\{\eta^5\text{-}1,2\text{-}C_5H_3(1,4\text{-}(R)_2N_2C_2\}]$ (**2a**–**3d**) were isolated by employing an off-metal ring closure route. Reacting thallium cyclopentadienide (Cp) salts (**1a**–**d**) with $[MBr(CO)_5]$ (M = Mn, Re) provided pyridazyl complexes (**2a**–**3d**) in high yield (75–99 %). Spectroscopic characterization (NMR, IR, MS) confirmed the identity of the desired organometallic pyridazines. The off-metal synthetic pathway employed did improve upon the isolation of these complexes as compared to previously reported routes. The molecular and electronic structure of complexes **2a**–**3d** and their optimal energy structures have been characterized with quantum chemistry calculations. Vibrational frequencies calculated were compared to their experimental counterparts. The excited state calculations predict that the dominant low-energy transition involves a ligand-to-metal charge transfer.

Introduction

Pyridazines and their derivative compounds have long been of interest in material applications due to their air and temperature stability [1]. Pyridazine compounds have been utilized in water reduction catalysis [2], the storage of hydrogen [3], chemiresistor sensors in TNT and DNT detection [4], as well as in the mimesis of α-helices [5]. In the context of our current investigation, we are primarily interested in the formation of organometallic pyridazines as building blocks for novel electronic devices (e.g., polymeric semiconductors). Devices made from these types of molecular materials offer the advantages of discounted production cost, increased processibility, as well as application to flexible substrates [6–8]. These unique properties are exemplified in commercial applications like Organic Light Emitting Diodes, Organic Photovoltaic Cells, and Organic Resistors [9–12]. The incorporation of metal moieties into these novel compounds is of additional interest, as the inclusion of a transition metal center allows for the ability to “tune” the electronic properties of the bulk material using the intrinsic redox properties of the metal. Specifically, Group VII metals exhibit a wide range of stable oxidation states (−1 through +7) and thus represent attractive, redox active candidates for incorporation. In addition, some rhenium (I) complexes have already been reported to possess luminescent properties, demonstrating their potential for electronic device applications. [13] Our recent research involves the synthesis and characterization of several organometallic 5,6-fused ring pyridazines. The synthetic route selected for the formation of our current pyridazyl series follows an off-metal ring closure of 1,2-diacylcyclopentadienes (fulvenes), as previously reported [14]. This pathway (Route 2) was employed, as opposed to the on-metal route pathway we previously investigated (Route 1) [15], due to the low yields and difficulties in

---

C. A. Snyder (✉) · J. B. Maddox · J. O. E. Young · B. D. Garabato · J. W. Evans · L. A. Dopierala · S. A. Shah · Z. A. Claytor · A. C. Smith
Department of Chemistry, Western Kentucky University, 1906 College Heights Blvd., Bowling Green, KY 42101, USA
e-mail: chad.snyder@wku.edu

N. C. Tice
Department of Chemistry, Butler University, 4600 Sunset Avenue, Indianapolis, IN 46208, USA

M. G. Mazzotta
Department of Chemistry, Purdue University, 560 Oval Drive, West Lafayette, IN 47907, USA

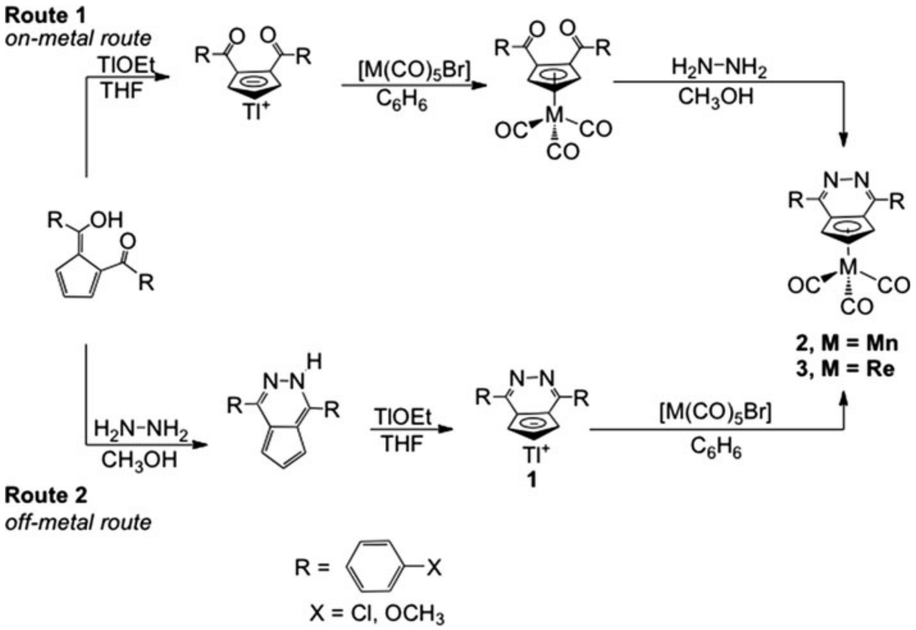

Scheme 1 Comparison of on- and off-metal routes of complexes **2**–**3**

isolation of some cases (Scheme 1). Thus, we hoped to not only expand the library of various substituted pyridazyl complexes available but to compare which of these two routes was the most facile in isolating the desired pyridazines. Herein is presented the synthesis, characterization, and electronic studies of various organometallic pyridazyl complexes.

Experimental

General procedures

All reactions were carried out using standard Schlenk techniques under a nitrogen atmosphere unless otherwise noted. NMR solvents acetone-d_6, DMSO-d_6, and $CDCl_3$ (Aldrich) were used without further purification. [MnBr(CO)$_5$] and [ReBr(CO)$_5$] (Strem) were used without further purification. All thallium Cp salt precursors were prepared according to literature methods [16–19]. Benzene was dried over sodium benzophenone ketyl.

^{1}H and ^{13}C NMR spectra were recorded on a JEOL-500 MHz NMR spectrometer at ca. 22 °C and were referenced to residual solvent peaks. All ^{13}C NMR spectra were listed as decoupled. Infrared spectra were recorded on a Spectrum One FT-IR Spectrometer. Electron ionization (EI) mass spectra were recorded at 70 eV on a Varian 500-MS Series LC/MS ion trap at Western Kentucky University's Advanced Materials Institute. Melting points were taken on a standard Mel-Temp apparatus. Elemental analyses were performed at Western Kentucky University's Advanced Materials Institute.

Synthesis of [Mn(CO)$_3${η^5-1,2-$C_5H_3(CC_6H_4BrN)(CC_6H_4BrN)$}] (**2a**)

In a 100-mL Schlenk flask, [MnBr(CO)$_5$] (94.3 mg, 0.344 mmol) was added to a stirred suspension of [Tl{1,2-C_5H_3(1,4-(4-Br)C_6H_4)$_2N_2C_2$}] (**1a**) (200 mg, 0.313 mmol) in 40 mL of dry benzene. The solution was then allowed to reflux gently for 3 h. The reaction mixture was cooled and passed through a thin pad (1 cm) of Celite, and the volatiles were removed in vacuo. Trituration with cold hexane afforded **2a** (134 mg, 0.238 mmol, 75.7 %) as a yellow powder. **Mp:** 135–157 °C. **^{1}H NMR (500 MHz, acetone-*d_6*, ppm):** δ 6.93 (t, 1H, ^3J = 2.9 Hz, CHC*H*CH), 7.30 (d, 1H, ^3J = 2.9 Hz, C*H*CHC*H*), 7.76 (d, 1H, ^3J = 7.4 Hz, C*H*CHCBr), 7.95 (d, 1H, ^3J = 7.4 Hz, CHC*H*CBr). **^{13}C NMR (125 MHz, acetone-*d_6*, ppm)**: δ 107.7 (CH*C*HCH), 120.4 (*C*HCH*C*H), 128.3, 130.8, 132.0, 132.5 (Ar), 154.7 (*C*N), 202.5 (MnCO). **IR (KBr, cm^{-1}):** 1,522 (C = N), 1,934, 2,027 (MnCO). **MS(EI-pos):** m/z 566 (M$^+$). Anal. Calcd. for $C_{22}H_{11}N_2Br_2O_3Mn$: C, 46.7; H, 1.9; N, 4.9. Found: C, 46.2; H, 1.9; N, 4.9.

Synthesis of [Re(CO)$_3${η^5-1,2-$C_5H_3(CC_6H_4BrN)(CC_6H_4BrN)$}] (**3a**)

In a 100-mL Schlenk flask, [ReBr(CO)$_5$] (314 mg, 0.772 mmol) was added to a stirred suspension of [Tl{1,2-C_5H_3(1,4-(4-Br)C_6H_4)$_2N_2C_2$}] (**1a**) (447 mg, 0.702 mmol) in 40 mL of dry benzene. The solution was then allowed to reflux gently for 3 h. The reaction mixture was cooled and passed through a thin pad (1 cm) of Celite, and the volatiles were removed in vacuo. Trituration with cold hexane afforded **3a** (388 mg, 0.554 mmol, 79.0 %) as a yellow powder. **Mp:** 157–162 °C. **^{1}H NMR (500 MHz, acetone-*d$_6$*, ppm):** δ 6.95 (d, 1H, ^3J = 3.4 Hz, C*H*CHC*H*), 7.41 (t, 1H, ^3J = 3.4 Hz, CHC*H*CH), 7.80 (d, 1H, ^3J = 8.0 Hz, C*H*CHCBr), 7.99 (d, 1H, ^3J = 8.0 Hz, CHC*H*CBr). **^{13}C NMR (125 MHz, DMSO-*d$_6$*, ppm)**: δ 107.7 (CH*C*HCH), 120.5 (*C*HCH*C*H), 130.7 (*C*CHCH), 132.0, 132.5 (Ph), 154.0 (*C*N) 179.2 (ReCO). **IR (KBr, cm^{-1}):** 1,589 (CN), 3,095 (CH), 2,003, 2,065 (ReCO). **MS(EI-pos):** m/z 698 (M$^+$). Anal. Calcd. for $C_{22}H_{11}N_2Br_2O_3Re$: C, 37.9; H, 1.6; N, 4.0. Found: C, 38.3; H, 1.7; N, 3.9.

Synthesis of $[Mn(CO)_3\{\eta^5\text{-}1,2\text{-}C_5H_3(CC_6H_4ClN)(CC_6H_4ClN)\}]$ (**2b**)

In a 100-mL Schlenk flask, $[MnBr(CO)_5]$ (186 mg, 0.458 mmol) was added to a stirred suspension of $[Tl\{1,2\text{-}C_5H_3(1,4\text{-}(4\text{-}Br)C_6H_4)_2N_2C_2\}]$ (**1b)** (500 mg, 0.923 mmol) in 40 mL of dry benzene. The solution was then allowed to reflux gently for 3 h. The reaction mixture was cooled and passed through a thin pad (1 cm) of Celite, and the volatiles were removed in vacuo. Trituration with cold hexane afforded **2b** (365 mg, 0.673 mmol, 83.0 %) as a yellow powder. **Mp**: 189–194 °C. **^{1}H NMR (500 MHz, CDCl$_3$, ppm):** δ 6.95 (br s, 1H, Cp), 7.39 (br s, 2H, Cp), 7.64–8.04 (m, 4H, Ar). **^{13}C NMR (125 MHz, CDCl$_3$, ppm)**: δ 92.4 (CH*C*HCH), 109.2 (*C*HCH*C*H), 121.0 (CC), 129.5, 129.9, 133.3, 137.4 (Ar), 156.5 (*C*N), 221.8 (Mn*C*O). **IR (KBr, cm^{-1}):** 1,597 (C = N), 1,949, 2,032 (MnCO). **MS(EI):** m/z 477 (M$^+$). Anal. Calcd. for $C_{22}H_{11}O_3N_2Cl_2Mn$: C, 55.3; H, 2.3; N, 5.9. Found: C, 60.8; H, 2.7; N, 6.6.

Synthesis of $[Re(CO)_3\{\eta^5\text{-}1,2\text{-}C_5H_3(CC_6H_4ClN)(CC_6H_4ClN)\}]$ (**3b**)

In a 100-mL Schlenk flask, $[ReBr(CO)_5]$ (206 mg, 0.507 mmol) was added to a stirred suspension of $[Tl\{1,2\text{-}C_5H_3(1,4\text{-}(4\text{-}Br)C_6H_4)_2N_2C_2\}]$ (**1b)** (250 mg, 0.461 mmol) in 40 mL of dry benzene. The solution was then allowed to reflux gently for 3 h. The reaction mixture was cooled and passed through a thin pad (1 cm) of Celite, and the volatiles were removed in vacuo. Trituration with cold hexane afforded **3b** (156 mg, 0.382 mmol, 83.0 %) as a yellow powder. **Mp:** 162–167 °C (dec). **^{1}H NMR (500 MHz, CDCl$_3$, ppm):** δ 7.05 (d, 2H, ^3J = 4.0 Hz, C*H*CHC*H*), 7.48 (d, 4H, ^3J = 8.0 Hz, C*H*CHCl), 7.54 (t, 1H, ^3J = 4.0 Hz, CHC*H*CH), 7.83 (d, 4H, ^3J = 8.0 Hz, CHC*H*Cl). **^{13}C NMR (125 MHz, CDCl$_3$, ppm)**: δ 109.3 (CH*C*HCH), 120.4 (*C*HCH*C*H), 129.4, 129.9, 133.4 (Ar), 176.2 (*C*N), 178.3 (Re*C*O). **IR (KBr, cm^{-1}):** 1,633 (C = N), 1,904, 2,028 (ReCO). **MS(EI):** m/z 338 (M$^+$ - Re(CO)$_3$). Anal. Calcd. for $C_{22}H_{11}O_3N_2Cl_2Re$: C, 43.4; H, 1.8; N, 4.6. Found: C, 31.7; H, 1.8; N, 2.3.

Synthesis of $[Mn(CO)_3\{\eta^5\text{-}1,2\text{-}C_5H_3(CC_6H_4CH_3N)(CC_6H_4CH_3N)\}]$ (**2c**)

In a 100-mL Schlenk flask, $[MnBr(CO)_5]$ (300 mg, 1.10 mmol) was added to a stirred suspension of $[Tl\{1,2\text{-}C_5H_3(1,4\text{-}(4\text{-}Br)C_6H_4)_2N_2C_2\}]$ (**1c**) (500 mg, 0.996 mmol) in 40 mL of dry benzene. The solution was then allowed to reflux gently for 3 h. The reaction mixture was cooled and passed through a thin pad (1 cm) of Celite, and the volatiles were removed in vacuo. Trituration with cold hexane afforded **2c** (324.9 mg, 0.745 mmol, 74.8 %) as a yellow powder. **Mp:** 192–207 °C. **^{1}H NMR (500 MHz, acetone-*d$_6$*, ppm):** δ 2.57 (s, 1H, CHCHCC*H$_3$*), 6.02 (d, 2H, ^3J = 2.9 Hz, C*H*CHC*H*), 6.36 (t, 1H, ^3J = 2.9 Hz, CHC*H*CH), 6.55 (d, 2H, ^3J = 7.5 Hz, CHC*H*CCH$_3$), 7.45 (d, 2H, ^3J = 7.5 Hz, C*H*CHCCH$_3$). **^{13}C NMR (125 MHz, DMSO-*d$_6$*, ppm)**: δ 24.5 (*C*H$_3$), 101.5 (CH*C*HCH), 120.0 (*C*HCH*C*H), 121.3 (*C*CHCH), 130.3, 132.6 (Ph), 153.1 (*C*N), 218.0 (MnCO). **IR** (Nujol, cm^{-1}): 1,601 (C = N), 1,929, 2,063 (MnCO). MS(EI):m/z 436 (M$^+$). Analysis Calc. for $C_{24}H_{17}O_3N_2Mn$: C, 66.1; H, 3.9. Found: C, 65.9; H, 4.2.

Synthesis of $[Re(CO)_3\{\eta^5\text{-}1,2\text{-}C_5H_3(CC_6H_4CH_3N)(CC_6H_4CH_3N)\}]$ (**3c**)

In a 100-mL Schlenk flask, $[ReBr(CO)_5]$ (186 mg,0.458 mmol) was added to a stirred suspension of $[Tl\{1,2\text{-}C_5H_3(1,4\text{-}(4\text{-}Br)C_6H_4)_2N_2C_2\}]$ (**1c**) (200 mg, 0.313 mmol) in 40 mL of dry benzene. The solution was then allowed to reflux gently for 3 h. The reaction mixture was cooled and passed through a thin pad (1 cm) of Celite, and the volatiles were removed in vacuo. Trituration with cold hexane afforded **3c** (223 mg, 0.444 mol, 99.0 %) as a yellow powder. Mp: 182–187 °C. **^{1}H NMR (500 MHz, acetone-*d$_6$*, ppm):** δ 2.42 (s, 1H, CHCHCC*H$_3$*), 5.97 (d, 2H, ^3J = 2.9 Hz, C*H*CHC*H*), 6.25 (t, 1H, ^3J = 2.9 Hz, CHC*H*CH), 6.63 (d, 2H, ^3J = 7.5 Hz, CHC*H*CCH$_3$), 7.25 (d, 2H, ^3J = 7.5 Hz, C*H*CHCCH$_3$). **^{13}C NMR (125 MHz, DMSO-d$_6$, ppm)**: δ 23.7 (*C*H$_3$), 100.2 (CH*C*HCH), 118.0 (*C*HCH*C*H), 122.7 (*C*CHCH), 129.7, 131.6 (Ph), 150.0 (*C*N), 183.4 (ReCO). IR (Nujol, cm^{-1}): 1,644 (C = N), 1,972, 2,052 (ReCO). MS(EI): m/z 568 (M$^+$). Analysis Calc. for $C_{24}H_{17}O_3N_2Re$: C, 50.8; H, 3.0. Found: C, 52.7; H, 4.3.

Synthesis of $[Mn(CO)_3\{\eta^5\text{-}1,2\text{-}C_5H_3(CC_6H_4OCH_3N)(CC_6H_4OCH_3N)\}]$ (**2d**)

In a 100-mL Schlenk flask, $[MnBr(CO)_5]$ (382 mg, 1.39 mmol) was added to a stirred suspension of $[Tl\{1,2\text{-}C_5H_3(1,4\text{-}(4\text{-}OCH_3)C_6H_4)_2N_2C_2\}]$ (**1d**) (978 mg, 1.95 mmol) in 60 mL of dry benzene. The solution was then allowed to reflux gently for 3 h. The reaction mixture was cooled and passed through a thin pad (1 cm) of Celite, and the volatiles were removed in vacuo. Trituration with cold hexane afforded **2d** (567 mg, 1.21 mmol 86.3 %) as a red powder. **Mp:** 160–170 °C. **^{1}H NMR (500 MHz, CDCl$_3$, ppm):** δ 5.29-5.39 (m, 3H, Cp), 5.52 (s, 6H, OCH_3), 7.53 (d, 4H, $^3J = 7.3$ Hz, Ar), 7.89 (d, 4H, $^3J = 7.30$ Hz, Ar). **^{13}C NMR (125 MHz, CDCl$_3$, ppm)**: δ 73.7 (OCH$_3$), 92.5 (CHCHCH), 109.1 (CHCHCH), 120.0 (CC), 129.5, 129.9, 133.4, 137.5 (Ar), 157.6 (CN), 220.1 (MnCO). **IR (KBr, cm^{-1}):** 1,608 (C = N), 1,932, 2,027 (MnCO). **MS(EI):** m/z 468 (M$^+$). Anal. Calcd. for $C_{24}H_{17}O_5N_2Mn$: C, 61.5; H, 3.6. Found: C, 60.9; H, 3.3.

Synthesis of [Re(CO)$_3${η^5-1,2-C$_5$H$_3$(CC$_6$H$_4$OCH$_3$N)(CC$_6$H$_4$OCH$_3$N)}] (**3d**)

In a 100-mL Schlenk flask, [ReBr(CO)$_5$] (186 mg, 0.458 mmol) was added to a stirred suspension of [Tl{1,2-C$_5$H$_3$(1,4-(4-Br)C$_6$H$_4$)$_2$N$_2$C$_2$}] (**2d**) (200 mg, 0.313 mmol) in 40 mL of dry benzene. The solution was then allowed to reflux gently for 3 h. The reaction mixture was cooled and passed through a thin pad (1 cm) of Celite, and the volatiles were removed in vacuo. Trituration with cold hexane afforded **3d** (228 mg, 0.369 mmol, 78.9 %) as a yellow powder. **Mp**: 212-221 °C. **^{1}H NMR (500 MHz, CDCl$_3$, ppm):** δ 3.90 (s, 6H, OCH_3), 7.00 (d, 4H, $^3J = 8.6$ Hz, NCCCH), 7.06 (d, 2H, $^3J = 4.0$ Hz, CHCHCH), 7.48 (t, 1H, $^3J = 4.0$ Hz, CHCHCH), 7.83 (d, 4H, $^3J = 8.6$ Hz, CHCHCO), 7.92 (d, 4H, $^3J = 8.6$ Hz, CHCHCO). **^{13}C NMR (125 MHz, CDCl$_3$, ppm)**: δ 55.4 (OCH$_3$), 108.9 (CHCHCH), 114.4 (CHCHCH), 120.3, 130.0, 132.0 (Ar), 161.1 (CN), 186.4 (ReCO). **IR (KBr, cm^{-1}):** 1,607 (C = N), 1,900, 2,014 (ReCO). **MS(EI):** m/z 602 (M$^+$), 330 (M$^+$ - Re(CO)$_3$). Anal. Calcd. for $C_{24}H_{17}O_5N_2Re$: C, 48.1; H, 2.9. Found: C, 49.0; H, 2.6.

Results and discussion

Synthesis and spectroscopic characterization

We have previously reported the on-metal synthesis (Route 1, Scheme 1) of a variety of group VII pyridazyl complexes [15]. In an effort to expand the number of available complexes and improve the percent yields and purity of these group VII pyridazyl complexes, we investigated the off-metal pathway (Route 2) for complexes **2a–3d**. The off-metal route differs from the on-metal by transmetalling with manganese or rhenium after the diacyl ring has been closed to the pyridazine. In a modification of a procedure by Wallace and Selegue [18], the thallium Cp salts **1** were generated by reaction of the free pyridazines (Scheme 1) with thallium (I) ethoxide. The general synthetic procedure for forming the target pyridazyl complexes **2** and **3** involved adding a slight excess (1.1–1.5 mmol) of metal carbonyl bromide ([M(CO)$_5$Br], M = Mn or Re) to a stirred solution of thallium Cp salt **1** in dry benzene. Each reaction solution was stirred under a gentle reflux for 3 h, cooled, filtered with Celite, and the organics were removed in vacuo. The crude product was triturated with hexane to yield complexes **2** and **3** in high yields, ranging from 75 to 99 %. Both the yields of manganese and rhenium complexes were comparable to one another, owing to their similar reactivity and stability. By comparison to the on-metal route, the percent yields for the target complex formation in the off-metal synthesis were improved by up to 23 % (**2b**). We also observed a modest increase in yield for complex **2d** (10 %). Conversely, there were only minor increases in percent yield for the rhenium cases **3b** and **3d**. Higher analytical purity was obtained for some target complexes. For example, elemental analysis for **3d** were significantly improved over the previously reported on-metal route [15]. The newly reported complexes **2a**, **3a**, **2c**, and **3c** each displayed a high degree of analytical purity with **3c** a minimal exception. We conclude that this observation is still likely the result of the lability on the pyridazyl ligand observed in other cases [15, 20]. Overall, the analytical purities were greatly improved employing the off-metal closure route (Scheme 2).

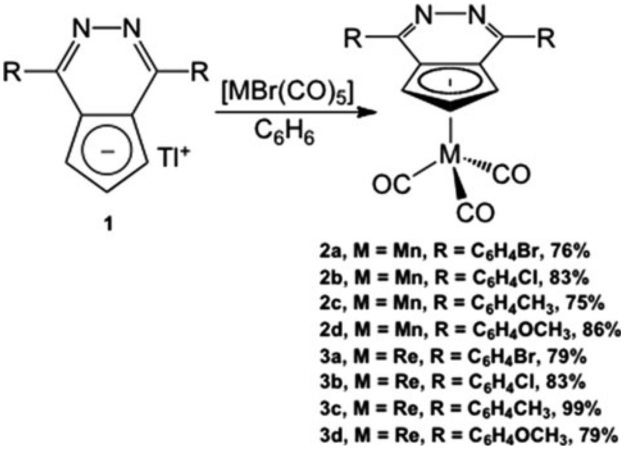

Scheme 2 Formation of complexes **2a–3d** via thallium Cp salts **1**

Manganese complexes **2a-d** and rhenium complexes **3a-d** were characterized using ^{1}H NMR, ^{13}C NMR, FT-IR, MS, and elemental analysis. Relevant spectroscopic data for all these complexes are reported here.

Table 1 shows pertinent Cp proton and carbon signals relevant to the characterization of complexes **2a–3d**. The ^{1}H NMR spectrum for [Mn(CO)$_3${η^5-1,2-C$_5$H$_3$(CC$_6$H$_4$BrN)-(CC$_6$H$_4$BrN)}] **(2a)** showed the expected doublet (7.30 ppm, $J = 2.9$ Hz) and triplet (6.93 ppm, $J = 2.9$ Hz), which corresponds to the Cp protons. These values match previously reported Cp chemical shifts, as well as corresponding

Table 1 Selected ^{1}H and ^{13}C NMR data for complexes **2a**–**3d**

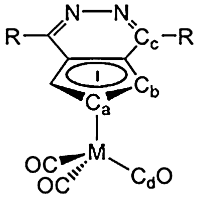

Complex	H_a	H_b	C_a	C_b	C_c	C_d
2a (M = Mn)	6.93 (t, $^{3}J = 2.9$ Hz)	7.30 (d, $^{3}J = 2.9$ Hz)	107.7	120.4	132.5	202.5
2b (M = Mn)	6.95 (br s)	7.39 (br s)	92.4	109.2	156.5	221.8
2c (M = Mn)	6.36 (t, $^{3}J = 2.9$ Hz)	6.02 (d, $^{3}J = 2.9$ Hz)	101.5	120.0	153.1	218.0
2d (M = Mn)	5.29–5.39 (m, 3H, Cp)	–	92.5	109.1	157.6	220.1
3a (M = Re)	7.41 (t, $^{3}J = 3.4$ Hz	6.95 (d, $^{3}J = 3.4$ Hz)	107.7	120.5	154.0	179.2
3b (M = Re)	7.54 (t, $^{3}J = 4.0$ Hz	7.05 (d, $^{3}J = 4.0$ Hz)	109.3	120.4	176.2	178.3
3c (M = Re)	6.25 (t, $^{3}J = 2.9$ Hz)	5.97 (d, $^{3}J = 2.9$ Hz)	100.2	118.0	150.0	183.4
3d (M = Re)	7.48 (t, $^{3}J = 4.0$ Hz)	7.06 (d, $^{3}J = 4.0$ Hz)	108.9	114.4	161.1	186.4

to **2c** (doublet at 7.30 ppm, $J = 2.9$ Hz and triplet 6.93 ppm, $J = 2.9$ Hz) [15]. Alternatively, manganese complex **2b** displayed two broad singlets at 6.95 and 7.39 ppm, owing to its Cp's triplet and doublet, respectively. Additionally, we observed a multiplet (in the range 5.29–5.39 ppm) that integrated to three protons for its Cp ring. Manganese complex **2d** also showed a singlet at 5.52 ppm as a result of the methoxy group, while the rhenium complex **3d** displayed its methoxy proton signal higher upfield at 3.90 ppm. As for rhenium complexes **3a–d** their spectra displayed the characteristic Cp doublet (ranging from 5.97 to 7.06 ppm) and triplet (ranging from 6.25 to 7.48 ppm). The average coupling constant for these Cp protons was 3.6 Hz, which was higher as compared to the average manganese Cp coupling constant (2.9 Hz). For Mn complexes **2a**, **2c**, and **2d**, the monosubstituted phenyl rings were observed as two doublets, ranging from 6.55–8.04 ppm. The average coupling constant for these complexes was 7.4 Hz. However, the chlorophenyl manganese complex **2b** displayed a multiplet from 7.64 to 8.04 ppm, but integrated to eight protons. Alternatively, two phenyl proton doublets were observed in each of the rhenium complexes having ranges of 6.63–7.83 ppm and 7.25–7.99 ppm (average $J = 8$ Hz).

The ^{13}C NMR spectra for all manganese complexes **2a**, **2b**, **2c**, and **2d** showed their Cp carbons, CH*C*HCH and *C*HCH*C*H, within the range of 92.4–107.7 ppm and 109.1–120.4 ppm, respectively (Table 1). Signals associated with the CH*C*HCH and *C*HCH*C*H shifts were similar in the rhenium cases, having values ranging between 100.2 and 109.3 ppm and 114.4–120.5 ppm, respectively. With the exception of rhenium complex **3b** (rhenium chlorophenyl complex), all organometallic complexes reported observed the C=N carbon chemical shifts between 150.0 and 161.1 ppm, as expected (**3b** C=N ~ 176 cm^{-1}). Finally, all Mn–CO carbon signals were found downfield (as previously reported) within the range of 202.5–221.8 ppm, whereas the Re–CO carbon signals were shifted more modestly upfield (178.3–189.9 ppm). This is in the range of previously reported Re–CO carbon shifts, which is likely the result of greater shielding from the 5d metal [16, 17, 19]. The IR spectroscopy (Table 2) and MS analysis also supported the formation of manganese and rhenium complexes **2a**–**3d**. The C=N stretch was observed between 1,522 and 1,644 cm^{-1}, with M–CO stretches observed in the expected ranges of 1,900–2,065 cm^{-1}. Each MS confirmed the molecular weight of each manganese (**2a**, $M^{+} = 566$ *m/z*; **2b**, $M^{+} = 477$ *m/z*; **2c**, $M^{+} = 436$ *m/z*; **2d**, $M^{+} = 468$ *m/z*) and rhenium complex (**3a**, $M^{+} = 698$ *m/z*; **3c**, $M^{+} = 568$ *m/z*; **3d**, $M^{+} = 602$ *m/z*). The rhenium chlorophenyl complex **3b** was the only case where an M^{+} signal was not observed in its MS. Instead, a signal was observed at 338 *m/z*, corresponding to

Table 2 Selected IR stretches for complexes **2a**–**3d**

Complex	CN (cm^{-1})	M(CO) (cm^{-1})	
		Exp.	Theory
2a	1,522	1,934, 2,027	1,864, 1,936
2b	1,597	1,949, 2,032	1,865, 1,937
2c	1,601	1,929, 2,063	1,861, 1,934
2d	1,608	1,932, 2,027	1,860, 1,934
3a	1,589	2,003, 2,065	1,871, 1,934
3b	1,633	1,904, 2,028	1,871, 1,934
3c	1,644	1,972, 2,052	1,867, 1,931
3d	1,607	1,900, 2,014	1,870, 1,930

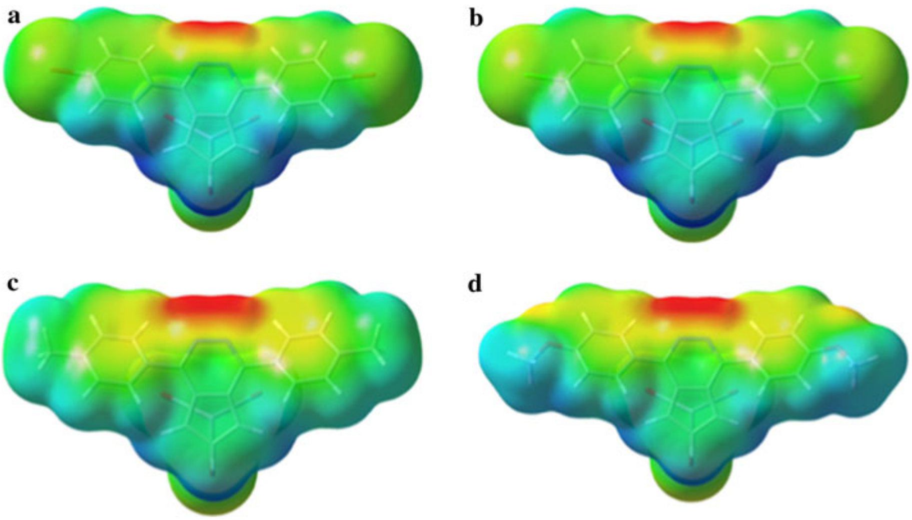

Fig. 1 Electron density isosurfaces mapped with electrostatic potentials for the rhenium complexes **3a**–**3d**. *Yellow* and *red regions* indicate electronegative regions of the molecule, while *light blue* and *blue regions* are electropositive. (Color figure online)

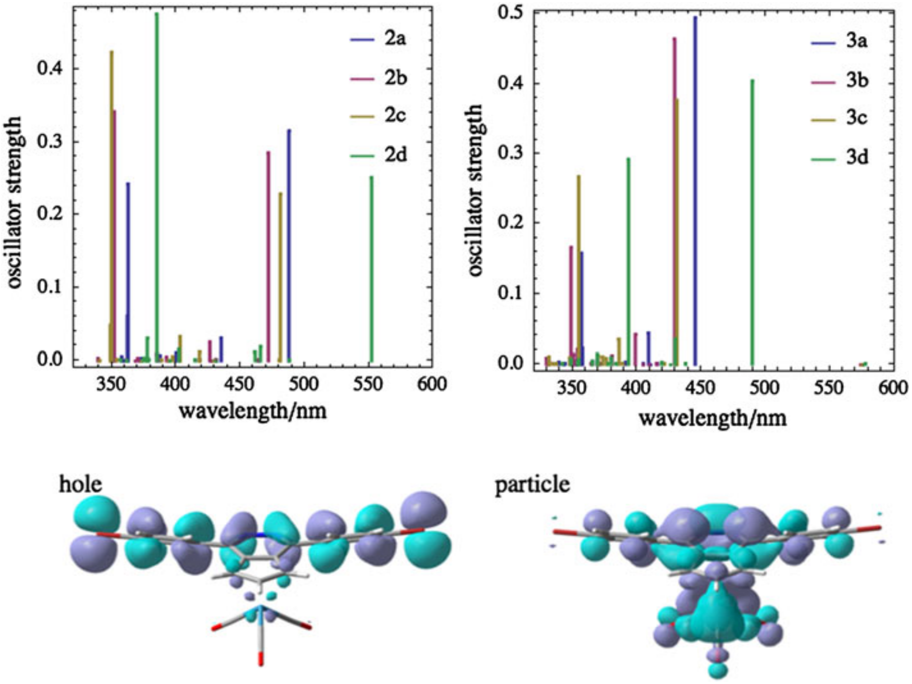

Fig. 2 (*Upper left*) Calculated wavelength versus oscillator strength for the optimized manganese complexes (*blue*) **2a**, (*red*) **2b**, (*yellow*) **2c**, and (*green solid*) **2d**. A modified conformer of compound **2d** is shown with *green dashed lines*. (*Upper right*) Calculated electronic transitions for the rhenium complexes **3a**–**3d**. (*Lower left*) NTO hole orbital for the dominant low-energy electronic transition at 445 nm in compound **3a**. (*Lower right*) Corresponding NTO particle orbital. (Color figure online)

the M$^+$– Re(CO)$_3$ signal. Finally, we attribute our inability to obtain analytically pure samples of complexes **2b, d** and **3c, d** to the lability of the pyridazine ligand [20]. Elemental analysis consistently gave higher than expected carbon values, consistent with the presence of a small amount of free pyridazine [20].

Electronic structure characterization

The molecular and electronic structures of complexes **2a**–**3d** have been characterized with density functional theory (DFT) and time-dependent DFT (TD-DFT) calculations using the Gaussian 09 quantum chemistry software [21]. Molecular geometry optimizations and normal mode calculations were carried out to obtain gas phase minimum energy molecular structures. These computations employed a model chemistry based on the Perdew-Burke-Ernzerhof (PBE) exchange–correlation functional [22, 23] and the Los Alamos double-zeta (lanl2dz) basis set [24–26]. The latter uses the Dunning/Huzinaga double zeta basis set [27] on light atoms and replaces core electrons on manganese and rhenium atoms with parameterized pseudopotential functions. It was found that the rhenium complexes (**3a**–**3d**) required tighter optimization cut-offs and an ultrafine

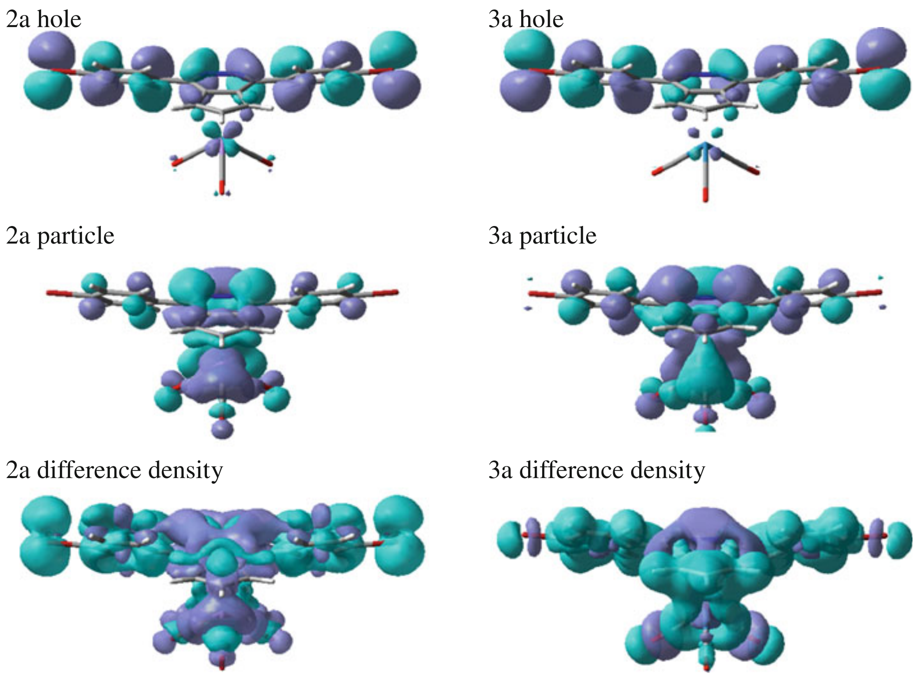

2a hole

3a hole

2a particle

3a particle

2a difference density

3a difference density

Fig. 3 (*Left*) Hole and particle NTOs and electronic difference density for the dominant low-energy electronic excitation of compound **2a**. (*Right*) NTOs and difference density for the dominant transition of compound **3a**

DFT integration grid in order to resolve the minimum energy conformation.

Electron density surfaces and electrostatic potential maps are shown in Fig. 1 for the optimized rhenium compounds **3a**–**3d**. Each compound shows a region of negative potential (yellow-to-red) concentrated near the two nitrogen atoms of the pyridazine rings. Likewise, all compounds exhibit slightly positive potential around the aromatic hydrogen atoms along the molecules' periphery. The methoxy oxygen atom in compound **3d** and the oxygen atoms on the carbonyl ligands for all compounds, which are not visible in Fig. 1, are also somewhat electronegative, as expected. The electron densities and electrostatic potential maps for the manganese complexes **2a**–**2d** exhibit similar features.

Normal mode frequency analysis confirmed that the optimized molecular structures were all local minima. Each compound displays a trio of predicted $M(CO)_3$ stretching modes with large IR activities. These include a symmetric stretch around 1,933–1,936 cm^{-1} and a pair of closely spaced asymmetric stretching modes in the ranges of 1,856–1,868 cm^{-1} and 1,864–1,873 cm^{-1}. We assign the symmetric stretch and the closely spaced pair to the two observed peaks discussed in the experimental section. The average frequency of the asymmetric pair and the frequency of symmetric stretch for compounds **2a**–**3d** are reported in Table 2. The calculations also predict that all compounds exhibit another vibrational mode with large IR activity in the range of 1,596–1,620 cm^{-1}. This vibration can be assigned to phenyl ring stretching in an out-of-phase fashion with respect to the two rings. Each compound exhibits a series of vibrational modes in the range of 1,350–1,500 cm^{-1}; the structure of these modes varies strongly from compound to compound and corresponds to delocalized stretching and distortion modes over all planar rings. Several of these modes include atomic displacements between carbon and nitrogen (i.e., C=N stretching); however, unique assignment of these modes to individual groups is not tractable.

We have also characterized several electronic transitions for all compounds using TD-DFT. The left and right panels of Fig. 2 show the calculated transition energies versus oscillator strengths (vertical colored lines) for the optimized molecular geometries of compounds **2a**–**2d** and **3a**–**3d**, respectively. Each species is predicted to have one dominant electronic transition with large oscillator strength at wavelengths >400 nm. For the manganese complexes **2a**, **2b**, and **2c,** this transition is found in the range of 472–488 nm. However, the calculated wavelength for the methoxy derivative **2d** is somewhat larger at 552 nm. The rhenium complexes follow a similar trend: the predicted wavelengths for the dominant low-energy electronic transition in compounds **3a**, **3b**, and **3c** occur in the range of 429–445 nm, while the dominant transition for compound **3d** is predicted at 490 nm.

A natural transition orbital (NTO) and difference density analysis of the low-energy electronic transition was carried out for all compounds [28].[1] There are no significant differences in the hole-particle orbital pairs or difference densities among the different analogs within the set of manganese and rhenium compounds. The left panels of Fig. 3 show the hole orbital, particle orbital, and difference density, respectively,

---

[1] NTO analysis is a useful tool for decomposing a given electronic transition in terms of hole-particle orbital pairs that assist with identifying the nature of the electronic transition.

for the dominant low-energy electronic transition in compound **2a**. The pattern exhibited by these NTOs is typical of the results obtained for all of the other manganese complexes. The hole orbital (top left) exhibits a characteristic π-bonding pattern and is delocalized over the pyridazine and phenyl rings. We note that the fulvene ring and the Mn(CO)$_3$ group do not significantly contribute to the electron density of the hole. The corresponding particle orbital (middle left) mainly involves electron density on the manganese atom and some anti-bonding character within the pyridazne and phenyl rings as well as on the carbonyl ligands. Again, the fulvene group does not appear to strongly participate in the particle orbital. Based on these observations, we attribute the low-energy electronic transition in complexes **2a**–**3d** to ligand-to-metal charge transfer (LMCT). The difference density (bottom left) provides additional confirmation; the blue portion represents the density of the hole, while the purple portion represents that of the particle. The difference density clearly shows that the excitation involves charge transfer from the phenyl rings to Mn(CO)$_3$ group.

The NTOs and difference density for the dominant low-energy electronic transition of compound **3a** are shown in the right panels of Fig. 3. The NTOs for 3a are very similar to those of compound **2a** and suggest that the excitation is also due to LMCT. However, the difference density shows that the excitation for **3a** involves a somewhat larger contribution from the fulvene ring to the hole and also a larger contribution from the pyridazine nitrogen atoms to the particle. In this sense, the amount of LMCT involved in **3a** appears to be less pronounced than in **2a**.

Overall, the electronic structure calculations corroborate the experimental IR characterization and provide qualitative assignment of the low-energy optical excitations as ligand-to-metal charge transfer. These pyridazyl compounds may provide a useful motif for initiating charge transfer in photovoltaic materials.

Conclusions

Formation and isolation of these fused ring pyridazine complexes (**2a**–**3d**) was accomplished under mild conditions and in good yields. By using an alternate synthetic pathway (off-metal ring closure route) for these complexes, isolation of the desired pyridazyl complexes were reported in higher yields as compared to the previously reported on-metal route. However, for some cases, we continued to observe the labile nature of the pyridazyl ligands. Our ongoing research efforts will focus upon the identification and isolation of these metal–pyridazine systems that demonstrate greater stability thereby offering greater potential for incorporation into real-world electronic devices.

Acknowledgments We would like to acknowledge our sources of financial support, including Western Kentucky University's Chemistry Department, their Office of Sponsored Programs, the WKU Faculty-Undergraduate Student Engagement (FUSE) grant, the WKU Research and Creative Activities Program (RCAP) grant, and the WKU Advanced Materials Institute.

References

1. Young JE (2012) Novel materials for use in homeland security research, M.S. Thesis, Department of Physics and Astronomy, Western Kentucky University, Bowling Green
2. Xu Y, Akermark T, Gyollai V, Zou D, Eriksson L, Duan L, Zhang R, Akermark B, Sun LC (2009) Inorg Chem 48:2717
3. Ghanem BS, Msayib KJ, McKeown NB, Harris KDM, Pan Z, Budd PM, Butler A, Selbie J, Book D, Walton A (2007) Chem Commun 1:67
4. Yang JS, Swager TM (1998) J Am Chem Soc 120:5321
5. Volonterio A, Moisan L, Rebek J (2007) Org Lett 9:3733
6. Wright ME, Sigman MS (1992) Macromolecules 25:6050
7. Zotti G, Zecchin S, Shiavon G (1995) Chem Mater 7:2309
8. Wisian-Neilson P, Allcock HR, Wynne KJ (eds) (1994) Inorganic and organometallic polymers II: advanced materials and intermediates ACS Symposium Series 572, Division of polymer chemistry, Inc.: Denver pp 442–497
9. Chandran D, Lee K (2013) Macromol Res 21:272
10. Su Y, Lan S, Wei K (2012) Mater Today 15:554
11. Guo Z, Zhu W, Tian H (2012) Chem Commun 48:6073
12. Lin Y, Li Y, Zhan X (2012) Chem Soc Rev 41:4245
13. Hock SJ, Schaper L, Herrmann WA, Kuhn FE (2013) Chem Soc Rev 42:5073
14. Young JOE, Snyder CA, Tice NC, Sloan SL, Smith AC, Shah SA, Dopierala LA, Crocker MS, Kobayashi Y, Mazzotta MG (2013) Syn Com 43:1
15. Tice NC, Snyder CA, Preston AZ, Wieliczko MB, Young JOE, Hinson DF (2012) Trans Met Chem 37:141
16. Snyder CA (2005) The synthesis, characterization, and structure of cyclopenta[*c*]thiophenes and their manganese complexes, Ph.D. Thesis, Department of Chemistry, University of Kentucky, Lexington
17. Tice NC (2006) The synthesis, structure, and reactivity of some organometallic—fused heterocycles. Ph.D. Thesis, Department of Chemistry, University of Kentucky, Lexington
18. Wallace CE, Selegue JP, Carrillo A (1998) Organometallics 17:3390
19. Snyder CA, Selegue JP, Tice NC, Wallace CE, Blankenbuehler MT, Parkin S, Allen KDE (2005) J Am Chem Soc 127:15010
20. Snyder CA, Tice NC, Maddox JB, Emberton ED, Vanover ES, Hinson DF, Jackson DC (2011) J Organomet Chem 696:2220
21. Gaussian 09, Revision A.02, M. Frisch MJ, Trucks GW, Schlegel HB, Scuseria GE, Robb MA, Cheeseman JA, Scalmani G, Barone V, Mennucci B, Petersson GA, Nakatsuji H, Caricato M, Li X, Hratchian HP, Izmaylov AF, Bloino J, Zheng G, Sonnenberg JL, Hada M, Ehara M, Toyota K, Fukuda R, Hasegawa J, Ishida M, Nakajima T, Honda Y, Kitao O, Nakai H, Vreven T, Montgomery JA Jr., Peralta JE, Ogliaro F, Bearpark M, Heyd JJ, Brothers E, Kudin KN, Staroverov VN, Kobayashi R, Normand, Raghavachari JK, Rendell A, Burant JC, Iyengar SS, Tomasi J, Cossi M, Rega N, Millam JM, Klene M, Knox JE, Cross JB, Bakken V, Adamo C, Jaramillo J, Gomperts R, Stratmann RE, Yazyev O, Austin AJ, Cammi R, Pomelli C, Ochterski JW, Martin RL, Morokuma K, Zakrzewski VG, Voth GA, Salvador P, Dannenberg JJ, Dapprich S, Daniels AD, Farkas Ö, Foresman JB, Ortiz

JV, Cioslowski J, and Fox DJ, Gaussian, Inc., Wallingford CT, 2009
22. Perdew JP, Burke K, Ernzerhof M (1996) Phys Rev Lett 77:3865
23. Ibid. (1997) 78:1396
24. Hay PJ, Wadt WR (1985) J Chem Phys 82:270
25. Wadt WR, Hay PJ (1985) J Chem Phys 82:284
26. Hay PJ, Wadt WR (1985) J Chem Phys 82:299
27. Dunning TH Jr, Hay PJ (1976) Modern theoretical chemistry. In: Schaefer III HF (ed) Plenum, vol 3. pp 1–28
28. Martin RL (2003) J Chem Phys 118:4775